Original Article

Institution of MECHANICAL ENGINEERS
Journal of AEROSPACE ENGINEERING

Proc IMechE Part G:
J Aerospace Engineering
0(0) 1–11

DOI: 10.1177/0954410016629692
uk.sagepub.com/jaero
SAGE

Altitude consensus based 3D flocking control for fixed-wing unmanned aerial vehicle swarm trajectory tracking

Xiangyin Zhang and Haibin Duan

Abstract

This paper studies the 3D flocking control problem for unmanned aerial vehicle swarm when tracking a desired trajectory. In order to allow the unmanned aerial vehicle swarm to form the stable flocking geometry on a same horizontal plane, the altitude consensus algorithm is applied to the unmanned aerial vehicle altitude control channel, using the trajectory altitude as the external input signals. The flocking control algorithm is only performed in the horizontal channel to control the horizontal position of unmanned aerial vehicles. The distributed tracking algorithm, which controls the local averages of position and velocity of each unmanned aerial vehicle, is implemented to achieve the better tracking performance. The improved artificial potential field method is introduced to achieve the smooth trajectory when avoiding obstacles. The practical dynamic and constraints of unmanned aerial vehicles are also taken into account. Numerical simulations are performed to test the performance of the proposed control algorithm.

Keywords

Unmanned aerial vehicle, swarm intelligence, flocking control, consensus, artificial potential field

Date received: 29 March 2015; accepted: 27 November 2015

Introduction

Flocking is a common phenomenon in nature, in which a large number of interacting agents, using only limited environmental information and simple rules, achieve fascinating collective behavior.[1,2] Prominent examples of collective motion are bird flocks, fish schools, and mammal herds.[3] Flocking problems have attracted much attention in various research fields, including biology, physics, control theory, and computer science for decades.[3-7] In 1986, Reynolds proposed the classical flocking model consisting of three heuristic rules:[8] (1) flock centering: attempt to stay close to nearby flockmates; (2) collosion avoidance: avoid collisions with nearby flockmates; and (3) velocity matching: attempt to match velocity with nearby flockmates. Based on the three rules, the flocking algorithms were proposed by a combination of velocity consensus and local artificial potential field (APF).[1,2,9-12]

The unmanned aerial vehicle (UAV) swarm-coordinated flight is similar to the collective behavior of bird flocks, fish schools, and sheep herds. In recent years, UAVs have been employed in both the military and civil applications more and more widely due to the improvement of the autonomy.[13] In addition to the research on the single UAV systems, there have been many studies on the coordinated control for the UAV swarm that aim to make a group of UAVs perform the missions cooperatively.[14-20] However, different from bird flocks, UAVs are allowed to fly at the same altitude in many real mission scenarios. In addition, the UAV swarm must have the ability to avoid obstacles in the environment. APF methods are the common approach to control UAVs to avoid obstacles. One drawback of the APF method is that it tends to result in oscillations when UAVs move near obstacles.

Consensus algorithms and their convergence analyses have recently been studied in various works.[21,22] Their applications to the UAV swarm area have also achieved much attention from researchers. The swarm

Bio-inspired Autonomous Flight Systems (BAFS) Research Group, School of Automation Science and Electrical Engineering, Beihang University, Beijing, PR China

Corresponding author:
Haibin Duan, Bio-inspired Autonomous Flight Systems (BAFS) Research Group, School of Automation Science and Electrical Engineering, Beihang University (BUAA), No. 37, Xueyuan Road, Haidian District, Beijing 100191, PR China.
Email: hbduan@buaa.edu.cn

controllers should consider the limitations of the UAV dynamics, including the velocity, heading angle, and altitude speed constraints. In this paper, we design the swarm-coordinated controller to allow UAVs to fly together along the desired trajectory. The UAV swarm 3D trajectory tracking problem is modeled as the flocking control issue in the horizontal channel and the altitude consensus issue in the vertical channel. The rest of his paper is organized as follows. The Model definition section describes dynamic model of the fixed-wing UAV used in our work. The Normal flocking control algorithms section presents the normal flocking control algorithm. The proposed altitude consensus based flocking algorithm is presented in the Altitude consensus-based swarm trajectory tracking algorithm section, including the improved APF method. The simulation test results are conducted in the Numerical simulations section. Finally, the Conclusions section gives the conclusions.

Model definition

This paper assumes that the UAV have inner-loop controls so only its controlled dynamics is of concern. With the UAV equipped with airspeed, heading, and altitude autopilots, the 12-dimensional state model of the UAV is reduced to a six-state model with velocity, heading angle and altitude command inputs.[23] Consider the UAV swarm system with N UAVs and let (x_i, y_i), h_i, ψ_i and V_i denote the inertial position, altitude, heading angle and forward velocity of the i-th UAV, respectively; the kinematic equations of motion are given as follows

$$\begin{aligned} \dot{x}_i &= V_i \cos\psi_i \\ \dot{y}_i &= V_i \sin\psi_i \\ \dot{V}_i &= \tfrac{1}{\tau_v}\left(V_i^{\mathrm{c}} - V_i\right) \\ \dot{\psi}_i &= \tfrac{1}{\tau_\psi}\left(\psi_i^{\mathrm{c}} - \psi_i\right) \\ \ddot{h}_i &= -\tfrac{1}{\tau_{\dot{h}}}\dot{h}_i + \tfrac{1}{\tau_h}\left(h_i^{\mathrm{c}} - h_i\right) \end{aligned} \tag{1}$$

where V_i^{c}, ψ_i^{c}, and h_i^{c} are the command inputs of velocity, heading angle, and altitude to the corresponding autopilots, respectively. The dynamics of the velocity and heading angle autopilots are modeled as first-order systems, while the altitude autopilot has the second-order dynamic characteristic. τ_v, τ_ψ, and $(\tau_{\dot{h}}, \tau_h)$ are the positive time constants for the velocity, heading angle, and altitude response with respect to the corresponding command inputs, respectively.

Considering the practical dynamic constraints of a real fixed-wing UAV, V_i, $\dot{\psi}_i$, and $\dot{h}_i$ should satisfy the following constraints

$$v_{\min} \leqslant V_i \leqslant v_{\max} \tag{2}$$

$$\left|\dot{\psi}_i\right| \leqslant n_{\max} g / V_i \tag{3}$$

$$\lambda_{\mathrm{glide}} \leqslant \dot{h}_i \leqslant \lambda_{\mathrm{climb}} \tag{4}$$

where $v_{\max}$, $v_{\min}$, $n_{\max}$, and λ_{climb} are positive constants that are the maximum velocity, the minimum velocity, the maximum lateral overload, and the maximum climbing speed, respectively. $\lambda_{\mathrm{glide}} < 0$ represents the maximum gliding speed. g is the gravitational acceleration. Due to the velocity constraints (2), the UAV can never stop or fly backwards.

Normal flocking control algorithms

This section presents the basic description of the flocking control algorithm. We consider a dynamic system of N agents (or particles) moving in an n-dimensional Euclidean space. The dynamics of each agent are modeled as the second-order integrators as follows

$$\begin{cases} \dot{\boldsymbol{q}}_i = \boldsymbol{p}_i \\ \dot{\boldsymbol{p}}_i = \boldsymbol{u}_i \end{cases}, i = 1, 2, \ldots n \tag{5}$$

where $\boldsymbol{q}_i$, $\boldsymbol{p}_i$, and $\boldsymbol{u}_i \in R^n$ denote the position, velocity, and control input vectors of the i-th agent, respectively. Each agent can only communicate with its neighbors within its communication region, and the neighboring set at time t is denoted as follows

$$N_i(t) = \left\{ j : \left\| \boldsymbol{q}_i - \boldsymbol{q}_j \right\| \leqslant r, j = 1, 2, \cdots, N, j \neq i \right\} \tag{6}$$

where $\| \cdot \|$ is the Euclidean distance and r is the interaction radius. The desired geometric model of flocks requires that each agent is equally distanced from all of its neighbors and satisfies the following constraints

$$\left\| \boldsymbol{q}_i - \boldsymbol{q}_j \right\| = d, \quad \forall i, j \in N_i(t) \tag{7}$$

where d is a positive constant indicating the distance between every pair of neighboring agents.

In the multi-obstacle environment, the control algorithm for flocking consists of three components as follow[1,2]

$$\boldsymbol{u}_i = \boldsymbol{f}_i^{\mathrm{f}} + \boldsymbol{f}_i^{\mathrm{o}} + \boldsymbol{f}_i^{\mathrm{n}} \tag{8}$$

where the three components $\boldsymbol{f}_i^{\mathrm{f}}$, $\boldsymbol{f}_i^{\mathrm{o}}$, and $\boldsymbol{f}_i^{\mathrm{n}}$ are used to control the agents to produce the flocking geometry, avoid the obstacles, and follow the navigation function, respectively. The first component $\boldsymbol{f}_i^{\mathrm{f}}$ consists of a velocity consensus term and a pair-wise attractive/repulsive action as follows

$$\boldsymbol{f}_i^{\mathrm{f}} = -c_1 \sum_{j \in N_i(t)} \left(\boldsymbol{p}_i - \boldsymbol{p}_j \right) - c_2 \sum_{j \in N_i(t)} \nabla_{\boldsymbol{q}_i} U^{\mathrm{f}}\left(\left\| \boldsymbol{q}_i - \boldsymbol{q}_j \right\| \right) \tag{9}$$

where c_1 and c_2 are two constant positive control gain. The second term of equation (9) is the gradient-based

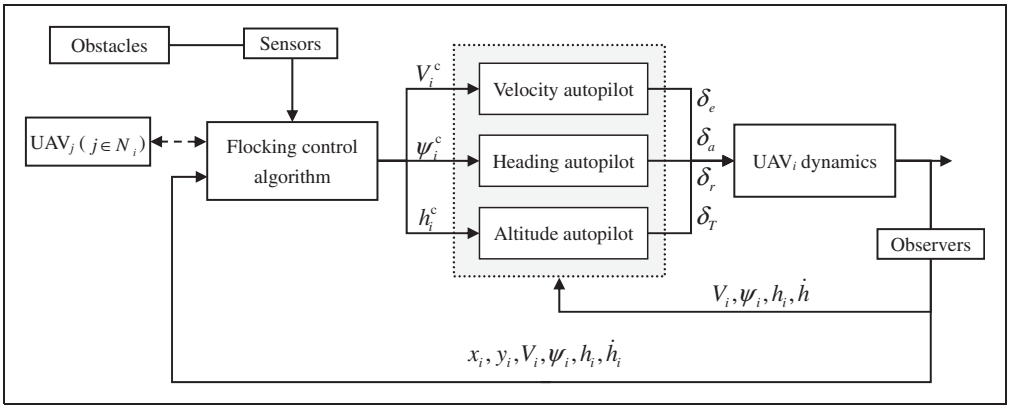

Figure 1. The block diagram of the flock control system for the UAV swarm.

component that allows each agent to maintain a certain distance from its neighbors and avoid collision with each other. The interaction potential function U^{f} depends only on the distance between the i-th and j-th agents, and is defined as[12]

$$U^{\mathrm{f}}(\|\mathbf{x}\|) = \frac{d^2}{\|\mathbf{x}\|^2} + \ln\|\mathbf{x}\|^2 \tag{10}$$

In order to avoid obstacles, the repulsive force $\boldsymbol{f}_i^{\mathrm{o}}$ is introduced to control the agent away from the obstacles, which is given by the negative gradient of the artificial potential function. One common used repulsive potential function takes the following form[17]

$$U_k^{\mathrm{o}}(\boldsymbol{q}) = \begin{cases} \frac{1}{2}\eta\left(\frac{1}{\rho(\boldsymbol{q},\boldsymbol{q}_k^{\mathrm{obs}})} - \frac{1}{\rho_0}\right)^2, & \rho(\boldsymbol{q},\boldsymbol{q}_k^{\mathrm{obs}}) \leqslant \rho_0 \\ 0, & \rho(\boldsymbol{q},\boldsymbol{q}_k^{\mathrm{obs}}) > \rho_0 \end{cases} \tag{11}$$

where η is a positive scaling factor, and $\boldsymbol{q}_k^{\mathrm{obs}}$ is the position of the point $\boldsymbol{q}$ projecting on the k-th obstacle, $\rho(\boldsymbol{q},\boldsymbol{q}_k^{\mathrm{obs}})$ is the minimal distance from $\boldsymbol{q}$ to the obstacle, and ρ_0 is the obstacle detection range.

The corresponding repulsive force is given by

$$\boldsymbol{f}_i^{\mathrm{o}} = -c_3 \sum_{k=1}^{n_{\mathrm{obs}}} \nabla_{\boldsymbol{q}_i} U_k^{\mathrm{o}}(\boldsymbol{q}_i) \tag{12}$$

where $c_3 > 0$ is the control gain and n_{obs} is the number of obstacles.

To control all agents to move together and track the virtual leader, the distributed navigational feedback term is introduced as follows

$$\boldsymbol{f}_i^{\mathrm{n}} = -c_4(\boldsymbol{p}_i - \boldsymbol{p}_{\mathrm{L}}) - c_5(\boldsymbol{q}_i - \boldsymbol{q}_{\mathrm{L}}) \tag{13}$$

where c_4 and c_5 are positive constants. $\boldsymbol{p}_{\mathrm{L}}$ and $\boldsymbol{q}_{\mathrm{L}}$ are the position and velocity of the moving target. If the virtual leader is moving in a given trajectory, all agents will track the trajectory together.

As to the UAV swarm system moving in the three-dimensional space, the position, velocity, and control vectors are $\boldsymbol{p}_i = [x_i, y_i, h_i]^T$, $\boldsymbol{q}_i = \left[V_i\cos\psi_i, V_i\sin\psi_i, \dot{h}_i\right]^T$, and $\boldsymbol{u}_i = \left[u_{x,i}, u_{y,i}, u_{h,i}\right]^T$. The relationships between the control vector $\boldsymbol{u}$ and the actual control command $\left[V_i^{\mathrm{c}}, \psi_i^{\mathrm{c}}, h_i^{\mathrm{c}}\right]$ are given by

$$V_i^{\mathrm{c}} = \tau_v\left(u_{x,i}\cos\psi_i + u_{y,i}\sin\psi_i\right) + V_i \tag{14}$$

$$\psi_i^{\mathrm{c}} = \frac{\tau_\psi}{V_i}\left(u_{y,i}\cos\psi_i - u_{x,i}\sin\psi_i\right) + \psi_i \tag{15}$$

$$h_i^{\mathrm{c}} = h_i + \frac{\tau_h}{\tau_{\dot{h}}}\dot{h}_i + \tau_h u_{h,i} \tag{16}$$

The flocking algorithm-based UAV swarm control system can be shown in Figure 1.

Altitude consensus-based swarm trajectory tracking algorithm

In this section, we build a framework of flocking control for the UAV swarm trajectory tracking based on altitude consensus and improved artificial potential field (APF) method. Our goal is to allow the whole UAV swarm to form the flocking geometry at the same altitude as the virtual leader. Therefore, as is illustrated in Figure 2, the control framework has two main parts, the altitude control module and the horizontal flight control module. The altitude control module uses the altitude consensus algorithm to provide the altitude autopilot with the command inputs, and all UAVs can fly in the same horizontal plane. The flocking control algorithm is applied to the horizontal fight control module, and it provides the velocity and heading autopilots with command inputs to allow the UAV swarm to keep the flight formation on the horizontal projection plane. With regard to the drawbacks of the APF method that it tends to result in oscillations when UAVs move near obstacles, the improved APF method is introduced to control the UAVs to avoid obstacles along the smoother routes. In addition, the distributed tracking algorithm, in which the local averages of position and velocity

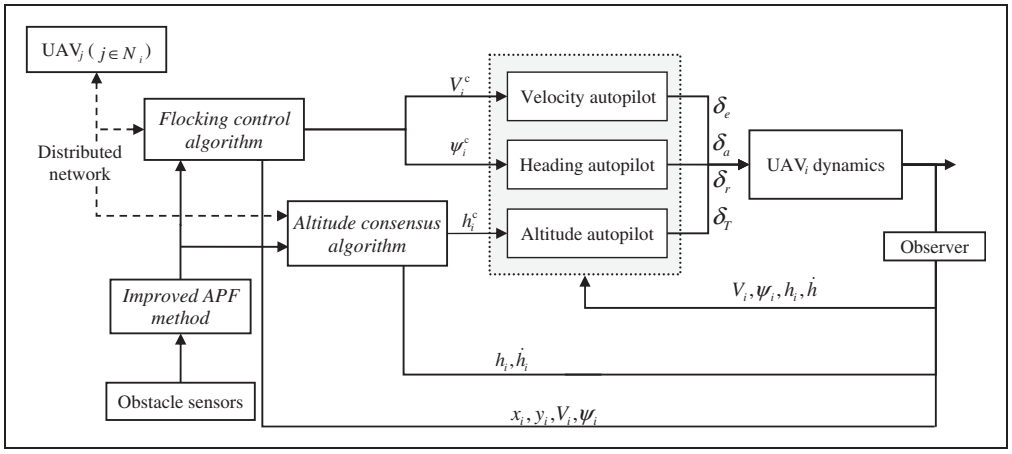

Figure 2. The block diagram of altitude consensus based flocking control system for the UAV swarm.

of each UAV are used to track the virtual leader, is implemented to achieve the better tracking performance.

Altitude consensus based flocking control algorithm

In order to allow the UAV swarm to keep the flock formation on the same horizontal plane, the UAV model is decoupled into the horizontal- and vertical-directional equations, and thus the swarm control strategies are considered separately. The horizontal state and control variables are $\boldsymbol{q}_i^{\mathrm{h}} = [x_i, y_i]^T$, $\boldsymbol{p}_i^{\mathrm{h}} = [\dot{x}_i, \dot{y}_i]^T$, and $\boldsymbol{u}_i^{\mathrm{h}} = [u_{x,i}, u_{y,i}]^T$, which have the following dynamic equations

$$\begin{cases} \dot{\boldsymbol{q}}_i^{\mathrm{h}} = \boldsymbol{p}_i^{\mathrm{h}} \\ \dot{\boldsymbol{p}}_i^{\mathrm{h}} = \boldsymbol{u}_i^{\mathrm{h}} \end{cases} \tag{17}$$

According to the distributed flocking control algorithm in equation (8), the horizontal flocking control law for the i-th UAV is designed as follows

$$\begin{aligned} \boldsymbol{u}_i^{\mathrm{h}} = & -c_p \sum_{j \in N_i(t)} \left(\boldsymbol{p}_i^{\mathrm{h}} - \boldsymbol{p}_j^{\mathrm{h}} \right) - c_q \sum_{j \in N_i(t)} \nabla_{\boldsymbol{q}_i} U^{\mathrm{f}} \left(\| \boldsymbol{q}_i^{\mathrm{h}} - \boldsymbol{q}_i^{\mathrm{h}} \| \right) \\ & - c_q^{\mathrm{l}} \left(\bar{\boldsymbol{q}}_{N_i \cup \{i\}}^{\mathrm{h}} - \boldsymbol{q}_{\mathrm{L}}^{\mathrm{h}} \right) - c_p^{\mathrm{l}} \left(\bar{\boldsymbol{p}}_{N_i \cup \{i\}}^{\mathrm{h}} - \boldsymbol{p}_{\mathrm{L}}^{\mathrm{h}} \right) + \boldsymbol{f}_i^{\mathrm{o}} \big|_{x,y} \end{aligned} \tag{18}$$

where c_p, c_q, c_q^{l}, and c_q^{l} are four positive constants. $\boldsymbol{f}_i^{\mathrm{o}} \big|_{x,y}$ is the horizontal component of the obstacle avoidance force. The local average information $\bar{\boldsymbol{q}}_{N_i \cup \{i\}}^{\mathrm{h}}$ and $\bar{\boldsymbol{p}}_{N_i \cup \{i\}}^{\mathrm{h}}$ of each UAV and its neighbors are controlled to track the given trajectory as follow[7]

$$\bar{\boldsymbol{q}}_{N_i \cup \{i\}}^{\mathrm{h}} = \frac{1}{1 + |N_i|} \sum\nolimits_{N_i \cup \{i\}} \boldsymbol{q}_i^{\mathrm{h}} \tag{19}$$

$$\bar{\boldsymbol{p}}_{N_i \cup \{i\}}^{\mathrm{h}} = \frac{1}{1 + |N_i|} \sum\nolimits_{N_i \cup \{i\}} \boldsymbol{p}_i^{\mathrm{h}} \tag{20}$$

where $|N_i|$ denotes the number of UAVs in the local neighboring region of the i-th UAV.

The vertical state and control variables of the i-th UAV are $\left(\dot{h}_i, h_i \right)$. Consider that the virtual leader moves along the desired trajectory with the dynamics $\left(\dot{h}_{\mathrm{L}}, h_{\mathrm{L}} \right)$, the altitude consensus control strategy is applied to guarantee that $\dot{h}_i \to \dot{h}_j \to \dot{h}_{\mathrm{L}}$, $h_i \to h_j \to h_{\mathrm{L}}$ as follow

$$\begin{aligned} u_{h,i} = & -c_{\dot{h}} \sum_{j \in N_i(t)} \left(\dot{h}_i - \dot{h}_j \right) - c_h \sum_{j \in N_i(t)} \left(h_i - h_j \right) \\ & - c_{\dot{h}}^{\mathrm{l}} \left(\dot{h}_i - \dot{h}_{\mathrm{L}} \right) - c_h^{\mathrm{l}} (h_i - h_{\mathrm{L}}) + \boldsymbol{f}_i^{\mathrm{o}} \big|_z \end{aligned} \tag{21}$$

where $c_{\dot{h}}$, c_h, $c_{\dot{h}}^{\mathrm{l}}$, and $c_{\dot{h}}^{\mathrm{l}}$ are positive constants. $\boldsymbol{f}_i^{\mathrm{o}} \big|_z$ is the vertical component of the obstacle avoidance force.

Improved obstacle avoidance algorithm

The traditional APF-based obstacle avoidance method usually allows the mobile agents to move towards the negative gradient direction of the corresponding potential field. However, when the agent is close to obstacles, the traditional APF method tends to result in serious oscillations. With regards to the dynamic constraints, UAVs cannot respond serious oscillations in the navigation direction so quickly to avoid obstacles. To overcome the problem of oscillations and achieve smoother routes, the modified Newton method (MNM) was introduced to improve the APF method in Ren et al.[24] In the MNM-based navigation algorithm, the agent is allowed to move along the Newton direction of the potential field. To achieve the better performance, the Levenberg-Marquardt (LM) algorithm was applied to the parameter adjusting in the MNM-based navigation algorithm. The thorough introduction to the LM-based navigation algorithm is in our prior work.[25] The following section gives a brief introduction of the technique.

Algorithm 1. Pseudo-code for the improved APF method to adjust ν.

Step 1: IF $\mathbf{G}+\nu\mathbf{I}$ is not positive-definite, THEN $\nu=4\nu$, go to Step 2,
ELSE $\nu=\nu/2$, go to Step 3.
Step 2: IF $\mathbf{G}+\nu\mathbf{I}$ is positive-definite, THEN go to Step 4, ELSE go to Step 1;
Step 3: IF $\mathbf{G}+\nu\mathbf{I}$ is not positive-definite, THEN $\nu=2\nu$, go to Step 4,
ELSE go to Step 1;
Step 4: Output ν and end adjusting.

The obstacle avoidance force term in equations (18) and (21) is designed as

$$\boldsymbol{f}_i^{\mathrm{o}}=-c_{\mathrm{o}}\sum_{k=1}^{n_{\mathrm{obs}}}\mathbf{B}(\boldsymbol{q}_i)\cdot\nabla_{\boldsymbol{q}_i}U_k^{\mathrm{o}}(\boldsymbol{q}_i) \tag{22}$$

where c_{o} is a positive constant. $\mathbf{B}(\boldsymbol{q}_i)=(\mathbf{G}+\nu\mathbf{I})^{-1}$ is a positive-definite matrix. $\mathbf{G}$ is the Hessian matrix of the potential function U^{o}, and ν is a positive parameter. In order to guarantee that the matrix $\mathbf{G}+\nu\mathbf{I}$ is always positive-definite, the parameter ν is adaptively adjusted according to the LM algorithm.[25] The adjusting steps of ν is illustrated in Algorithm 1.

Numerical simulations

In this section, we present several simulation results of the 3D trajectory tracking for the UAV swarm. The basic flocking control algorithm (8) and the altitude consensus-based flocking algorithms (18) and (21) are tested in both two scenarios. All the algorithms are implemented using a 3.07GHz CPU and 4G memory personal computer running Windows 7 and Matlab R2009a. The step-size in all simulations is Δt=0.025 s. Controlled objects used in simulations are the swarm consisting of $N=20$ small fixed-wing UAVs, of which the relevant parameters are listed in Table 1. Initial positions of all UAVs are set randomly from the box $[-40, 40]\times[-40, 40]\times[90, 110]$, and the initial motion states are set randomly as $V_i(0)\in[5, 15]$, $\psi_i(0)\in[-\pi,\pi]$, and $\dot{h}_i(0)=0$. The desired trajectory starts at the point $\boldsymbol{q}_{\mathrm{L}}(0)=[20, 0, 100]^T$. The parameter values of the control algorithms used in the simulation are summarized in Table 2.

To analyze the connectivity of the UAV swarm, the graph Laplacian matrix is defined as follows

$$L=D-A \tag{23}$$

where $A=[a_{ij}]$ is the adjacency matrix that is defined as

$$a_{ij}=\begin{cases}1, & \text{if } j\in N_i(t)\\ 0, & \text{otherwise}\end{cases} \tag{24}$$

Table 1. Model parameters for the UAV dynamics.

Parameter	Notation	Value
Velocity time constant	τ_v	5
Heading angle time constant	τ_ψ	0.75
Altitude time constant	$[\tau_h, \tau_h]$	[0.3, 1]
Minimum and maximum velocity (unit: m/s)	$[v_{\min}, v_{\max}]$	[5, 15]
Maximum lateral overload (unit: g)	$n_{\max}$	5
Maximum climbing and gliding velocity (unit: m/s)	$[\lambda_{\mathrm{climb}}, \lambda_{\mathrm{glide}}]$	[−5, 5]

Table 2. Parameters used in the simulations.

Parameter	Notation and value
Interaction radius	$r=25$
Desired distance between neighboring UAVs	$d=20$
Control gains of the algorithm (8)	$c_1=1$, $c_2=4$, $c_3=1$, $c_4=1$, $c_5=2$
Parameters of the repulsive potential function (11)	$\eta=100$, $\rho_0=20$
Control gains of the algorithm (18)	$c_p=1$, $c_q=4$, $c_q^l=1$, $c_q^l=2$
Control gains of the algorithm (21)	$c_h=1$, $c_h=2$, $c_h^l=1$, $c_h^l=2$

and $D=\mathrm{diag}(d_1, d_2, \cdots, d_N)$ with $d_i=\sum_{j=1, j\neq i}^{N}a_{ij}$. L is a symmetric matrix with real eigenvalues, and the set of eigenvalues of L can be ordered sequentially in an ascending order as

$$0=\lambda_1\leqslant\lambda_2\leqslant\cdots\leqslant\lambda_n \tag{25}$$

where the second smallest eigenvalue $\lambda_2\geqslant 0$ of Laplacian matrix is called the algebraic connectivity, which is a measure of performance/speed of consensus algorithms.[21]

Case 1. Tracking the line trajectory at the fixed velocity

In this simulation, the desired trajectory is a rectangle with jumping altitude and UAVs track trajectory at the fixed velocity. Figure 3 shows the 3D and 2D simulation results of tracking for UAVs using the normal flocking control algorithm and the altitude consensus-based flocking algorithm. In the figures, each UAV is represented by an equilateral triangle, of which the apex angle points to the direction of motion. The red lines represent the desired trajectory, while the blue lines represent the actual trajectory of the swarm average position. The thin lines between UAVs represent the communication network among neighboring UAVs. It can be seen that our proposed

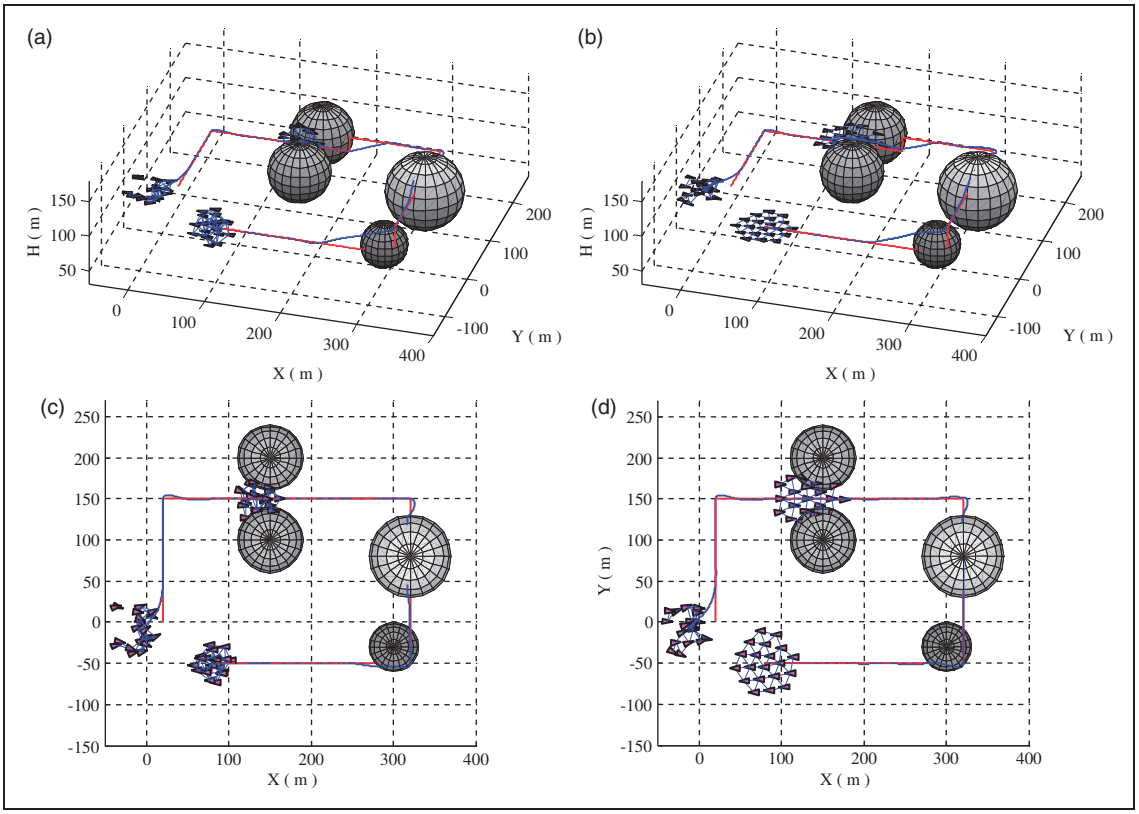

Figure 3. Snapshots of the motion of UAVs at the beginning ($t = 0$s), avoiding obstacles ($t = 25$s) and at the ending ($t = 80$s) when they are tracking the line trajectory using the normal 3D flocking control algorithm (a, c) and the altitude based flocking algorithm (b, d). (c) and (d) are the plan views of (a) and (b) onto the horizontal plane, respectively.

altitude consensus-based flocking control algorithm allows the UAV swarm to keep level flight on the desired altitude, and the swarm of UAVs form the flocking geometry on the same horizontal plane.

The motion state histories of each UAV and the virtual leader are displayed in Figure 4, including the velocity, heading angle, altitude, and the speed of altitude. With the altitude consensus algorithm, UAVs maintain the formation at the same altitude with the leader. When the altitude step changing of the leader or the obstacle avoidance disrupt the consensus state, UAVs can always reach a consensus on the flight altitude and return to the desired trajectory quickly. Compared to the heading angle response curves in Figure 4(c) and (d), oscillations of (d) are weaker than those of (c), which indicates that, when flying close to obstacles, the improved APF method achieve smoother routes and have the better performance than the basic APF method in terms of oscillations.

In order to compare quantitatively the oscillations degree of the two algorithms, the average maneuvering parameter $\bar{\kappa} = \sum_t \kappa(t)$ is introduced to synthetically consider the change rate in the heading and altitude of all UAVs, where

$$\kappa(t) = \sum_{i=1}^{N} \frac{|\Delta\psi_i(t)|}{(n_{\max} g / V_i(t))\Delta t} + \sum_{i=1}^{N} \frac{|\Delta h_i(t)|}{\dot{h}_{\max}\Delta t} \tag{26}$$

Table 3. Quantitative comparisons.

		$\bar{\kappa}$	$\bar{e}_{\mathbf{q}}$	$\bar{e}_h$	Λ
Case 1	Normal method	0.32	4.57	4.76	92.91%
	Proposed method	0.30	3.80	5.49	98.00%
Case 2	Normal method	0.20	2.79	1.66	98.28%
	Proposed method	0.17	1.70	1.88	99.09%

Table 3 shows the values of $\bar{\kappa}$ using the two algorithms in the simulations of Case 1. The proposed algorithm has the smaller value of $\bar{\kappa}$ than the normal algorithm and it indicates that the improved APF method can help to achieve the smoother route from the angle of quantification.

The swarm tracking errors of UAVs can be shown in Figure 5, including the position error $e_{\boldsymbol{q}} = \left\| \langle \boldsymbol{q} \rangle - \boldsymbol{q}_{\mathrm{L}} \right\|$ and altitude error $e_h = |\langle h \rangle - h_{\mathrm{L}}|$, where $\langle \boldsymbol{q} \rangle = \frac{1}{N}\sum_{i=1}^{N} \boldsymbol{q}_i$ and $\langle h \rangle = \frac{1}{N}\sum_{i=1}^{N} h_i$. We can see that the results of tracking performance in Figure 5(b) and (d) using the altitude consensus-based flocking algorithm are better than those in Figure 5(a) and (c) using the normal flocking algorithm. The average tracking errors of the horizontal position and the altitude $\bar{e}_{\boldsymbol{q}}$, $\bar{e}_h$ using the two algorithms are listed in Table 3. The proposed

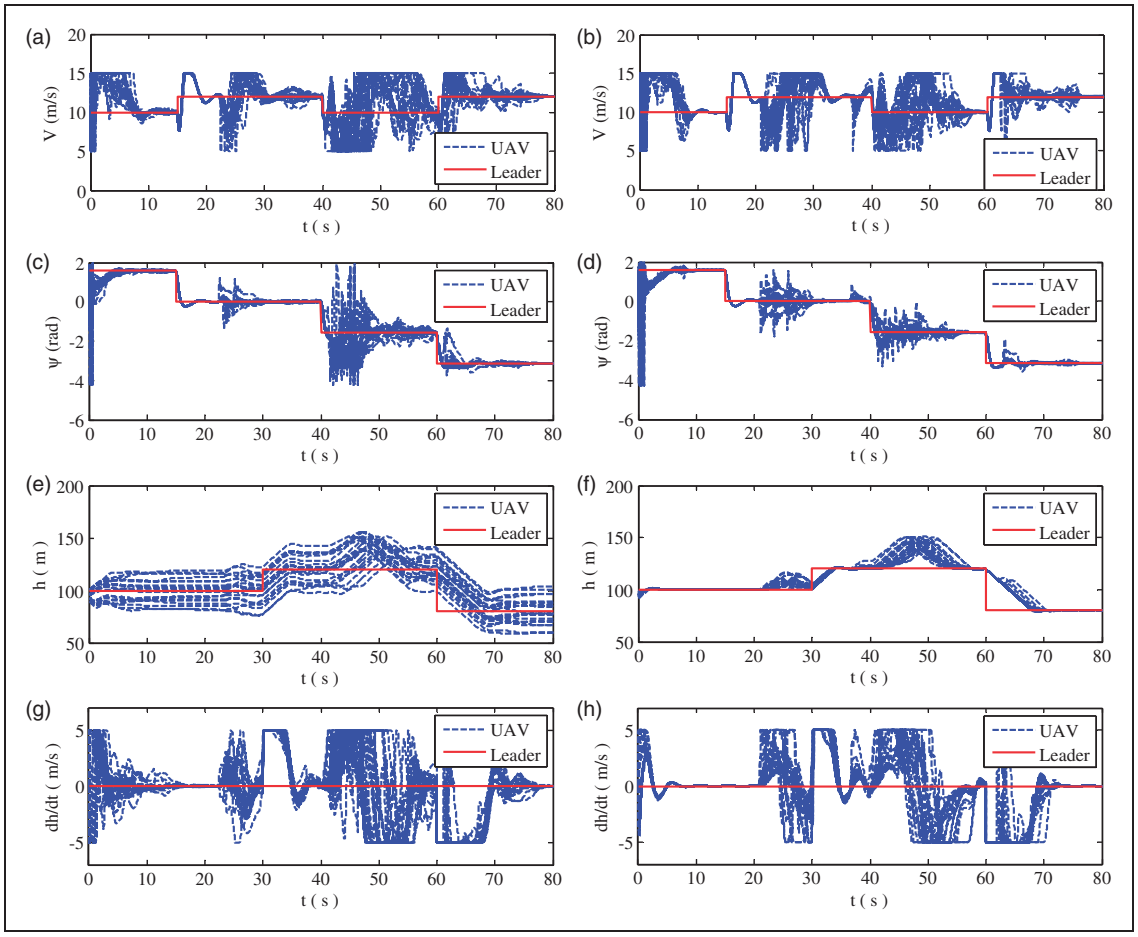

Figure 4. The time response of velocity, heading angle, altitude, and the speed of altitude for each UAV and the virtual leader when tracking the line trajectory at a fixed velocity. (a, c, e, g) are the results using the normal flocking algorithm, and (b, d, f, h) are the results using the altitude consensus based flocking algorithm.

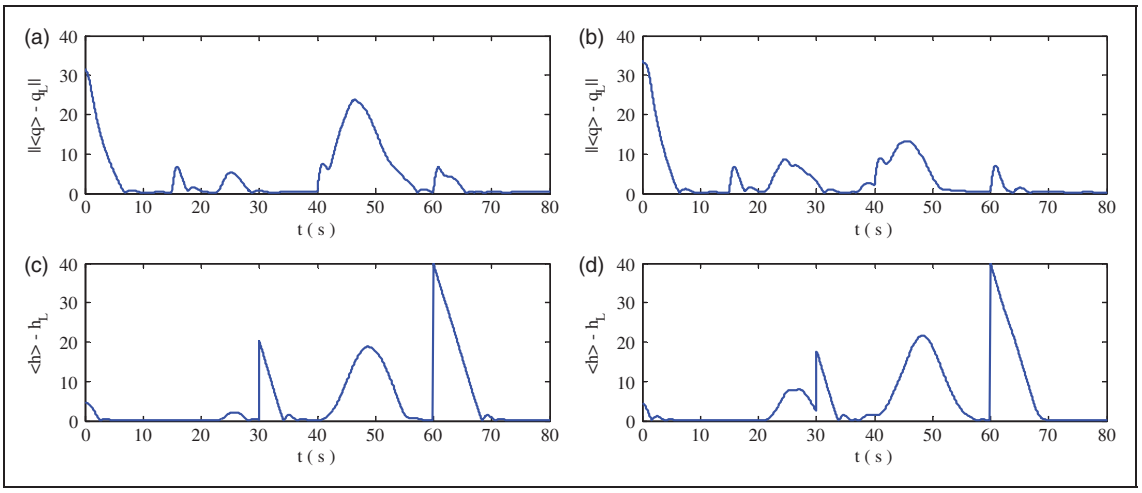

Figure 5. Tracking error curves between the UAV swarm and the desired trajectory when they are tracking the line trajectory. $\langle \mathbf{q} \rangle$ and $\langle h \rangle$ represent the average position and altitude of UAVs, respectively. (a) and c) are the results using the normal flocking algorithm, and (b) and (d) are the results using the altitude consensus based flocking algorithm.

altitude consensus based flocking algorithm has the smaller tracking error in the horizontal position but bigger error in the altitude. Results of the algebraic connectivity of the UAV swarm are shown in Fig. 6. Though the network in UAVs is broken ($\lambda_2 = 0$) when avoiding obstacles, the UAV swarm can repair the communication topology and remain connected when leaving the obstacle spaces. The parameter

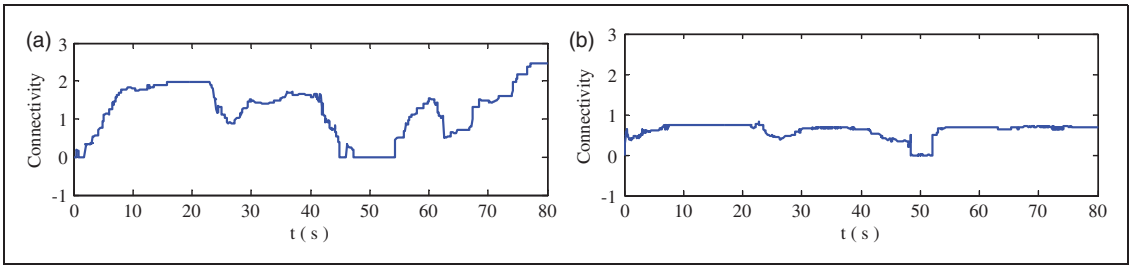

Figure 6. Algebraic connectivity of the UAV swarm when tracking the line trajectory using (a) the normal flocking algorithm and (b) the altitude consensus-based flocking algorithm.

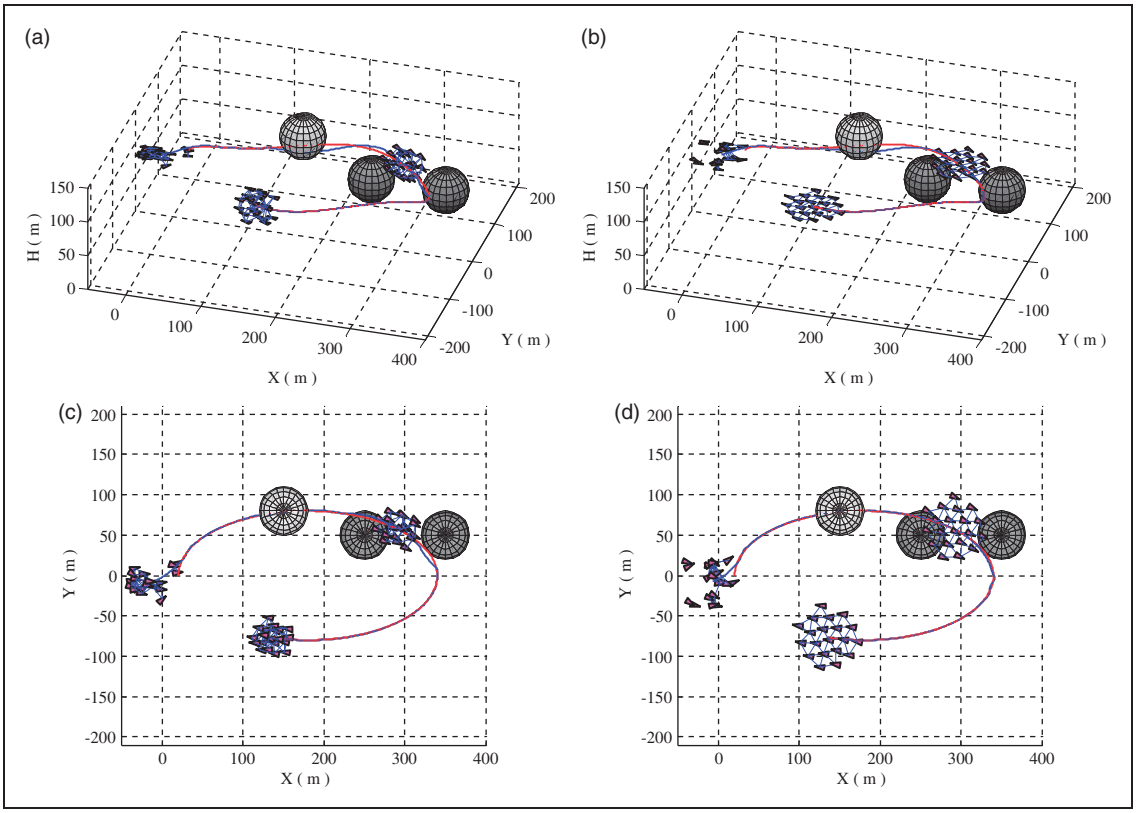

Figure 7. Snapshots of the motion of UAVs at the beginning ($t = 0$ s), avoiding obstacles ($t = 50$ s) and at the ending ($t = 80$ s) when they are tracking the elliptical trajectory. Here, (a) and (c) are the results using the normal 3D flocking control algorithm, while (b) and (d) are the results using the altitude based flocking algorithm. (c) and (d) are the plan views of (a) and (b) onto the horizontal plane, respectively.

$\Lambda = \frac{t_{\lambda>0}}{t_{\max}} \times 100\ \%$, where $t_{\lambda>0}$ denotes the time that the communication topology is connected with $\lambda_2 > 0$ and $t_{\max}$ is the total simulation time, is introduced to measure the scale of the connected time of communication topology during the simulation. The last row of Table 3 shows the values of Λ for the simulation in Case 1. It can be seen that the proposed altitude consensus-based flocking algorithm can allow the UAV swarm to remain connected during longer time.

Case 2. Tracking elliptical trajectory at the time-varying velocity

In this simulation, we assume the desired trajectory is an elliptical shape and UAVs are allowed to track trajectory at the time-varying velocity. The parameters are the same as those in Case 1, and the virtual leader flies at the velocity $\boldsymbol{p}_{\mathrm{L}}(t) = [10\sin(t/16),\ 5\cos(t/16),\ -2\sin(t/5)]^T$. The normal flocking algorithm and our proposed algorithm are both implemented for comparison. The actual motion trajectories of the UAV swarm are displayed in Figure 7. The corresponding state response and tracking error curves are shown in Figures 8 and 9. Figure 10 shows the algebraic connectivity of the UAV swarm. The quantitative comparison of the two algorithms in Case 2 is listed in Table 3. From the simulation results, it can be seen that both the two flocking algorithms can track the desired trajectory with the desired velocity, but our proposed algorithm can achieve the better tracking performance with smoother trajectory.

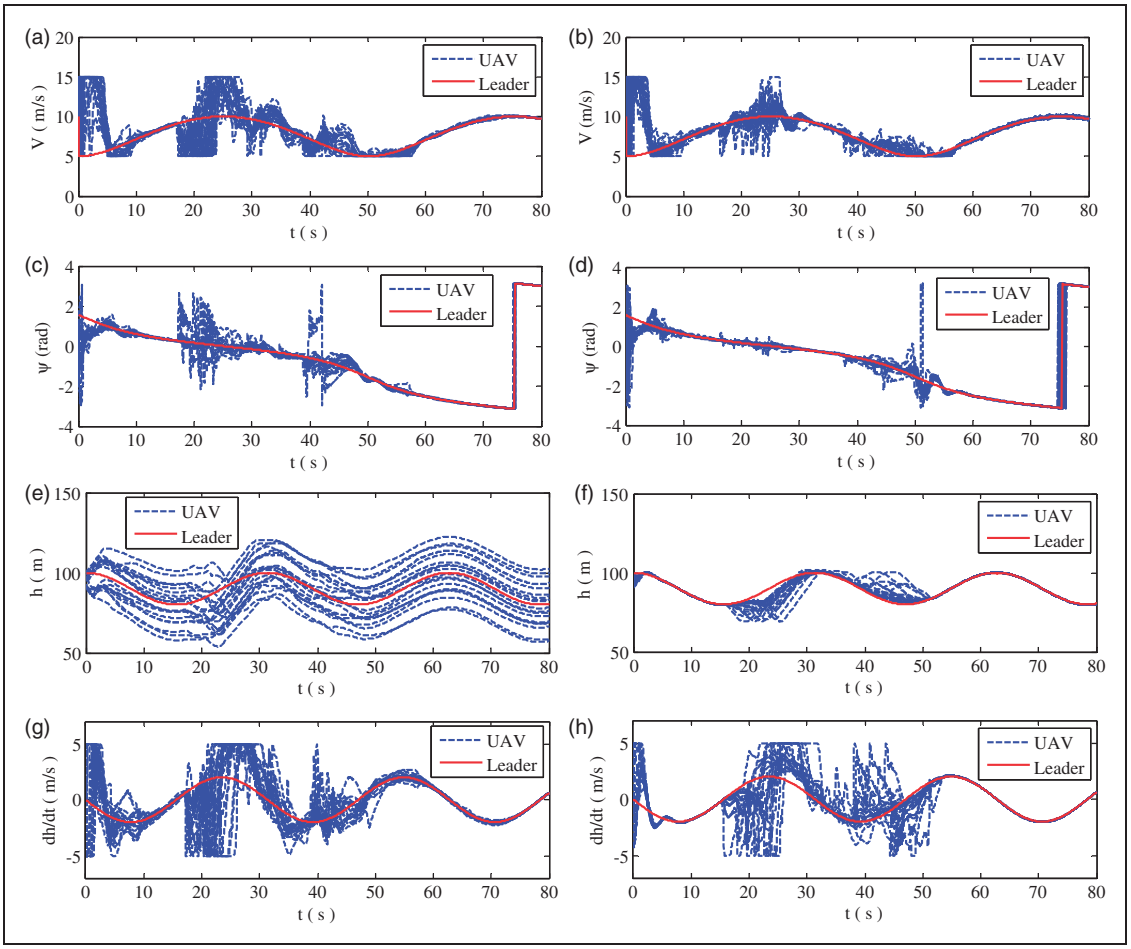

Figure 8. The time response of velocity, heading angle, altitude, and the speed of altitude for each UAV and the virtual leader when tracking the elliptical trajectory at time-varying velocity. (a), (c), (e), and (g) are results using the normal flocking algorithm, and (b), (d), (f), and (h) are results using the altitude consensus-based flocking algorithm.

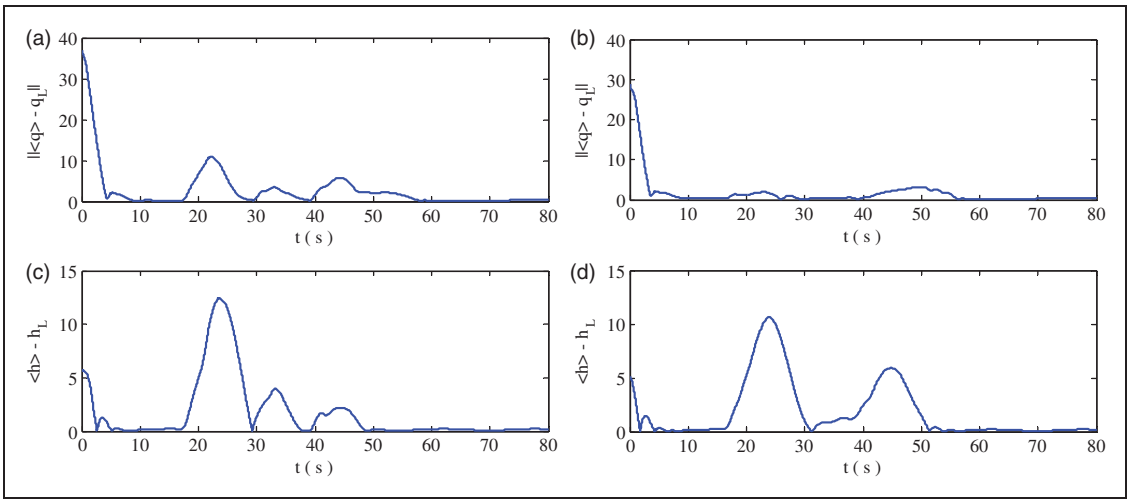

Figure 9. Tracking error curves between the UAV swarm and the desired trajectory when they are tracking the elliptical trajectory. $\langle \mathbf{q} \rangle$ and $\langle h \rangle$ represent the average position and altitude of UAVs, respectively. (a) and (c) are the results using the normal flocking algorithm, and (b) and (d) are the results using the altitude consensus-based flocking algorithm.

In all the above simulation results, all UAVs satisfy their dynamic constraints. The UAV swarms keep the flocking formation on the same altitude and no collision occurs among them using the proposed flocking algorithm, and they avoid obstacles without serious and redundant maneuvering using the improved APF method.

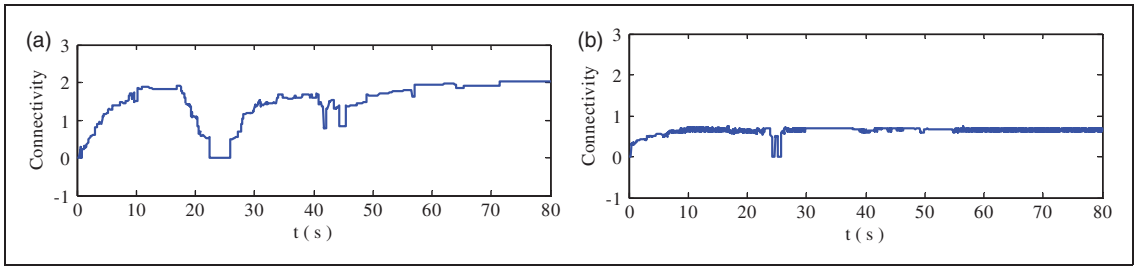

Figure 10. Algebraic connectivity of the UAV swarm when tracking the elliptical trajectory using (a) the normal flocking algorithm and (b) the altitude consensus-based flocking algorithm.

Conclusions

In this paper, we study the trajectory tracking problem of the UAV swarm in 3D environment. We assume the fixed-wing UAV is equipped with airspeed, heading, and altitude autopilots in this paper and several practical dynamic constraints of UAVs are also taken into account. Considering the special mission requirement of UAVs, we design the UAV swarm control problem satisfying (1) UAVs form the flocking geometry and (2) UAVs fly at the same altitude. To solve the problem, we proposed the altitude consensus based flocking control algorithm for the UAV swarm. The altitude consensus algorithm is used to allow all UAVs to fly in the same horizontal plane, while the flocking control algorithm is applied to the horizontal fight module to keep the flight formation on the horizontal projection plane. In addition, the improved APF method is introduced to control the UAVs to avoid obstacles without serious oscillations. Several simulations are performed using the normal flocking control algorithm and the proposed altitude consensus based flocking algorithm to solve the 3D trajectory tracking for the UAV swarm. Two simulation scenarios are tested, including the line trajectory tracking at a fixed velocity and the elliptical trajectory tracking at the time-varying velocity. Simulation results show that our proposed algorithm can achieve the good tracking performance with smooth trajectory and the UAV swarm can keep the stable flocking formation without avoiding obstacles. This approach cannot only be useful in dealing with the UAV swarm tracking problem but also be applicable to unmanned ground vehicles (UGVs), autonomous underwater vehicles (AUVs), missiles, and so on. In the future, we will investigate the stability of the proposed algorithms.max

Declaration of conflicting interests

The author(s) declared no potential conflicts of interest with respect to the research, authorship, and/or publication of this article.

Funding

The author(s) disclosed receipt of the following financial support for the research, authorship, and/or publication of this article: This work was partially supported by the National Natural Science Foundation of China under grant nos 61425008, 61333004 and 61273054 and the Aeronautical Foundation of China under Grant no. 2015ZA51013.

References

1. Olfati-Saber R. Flocking for multi-agent dynamic systems: algorithms and theory. *IEEE Transact Automat Ctrl* 2006; 51: 401–420.
2. Su H, Wang X and Lin Z. Flocking of multi-agents with a virtual leader. *IEEE Transact Automat Ctrl* 2009; 54: 293–307.
3. Vicsek T and Zafeiris A. Collective motion. *Phys Rep* 2012; 517: 71–140.
4. Vicsek T, Cziroók A, Ben-Jacob E, et al. Novel type of phase transition in a system of self-driven particles. *Phys Rev Lett* 1995; 75: 1226–1229.
5. Zhang YP, Duan HB and Zhang XY. Stable flocking of multiple agents based on potential field and distributed receding horizon control. *Chinese Phys Lett* 2011; 28: 040503-4.
6. Wang ZY and Gu DB. Cooperative target tracking control of multiple robots. *IEEE Transact Industrial Electron* 2012; 59: 3232–3240.
7. La HM, Lim R and Sheng W. Multirobot cooperative learning for predator avoidance. *IEEE Transact Ctrl Syst Technol* 2015; 23: 53–63.
8. Reynolds CW. Flocks, herds, and schools: a distributed behavioral model. *Comput Graph* 1987; 21: 25–34.
9. Tanner HG, Jadbabaie A and Pappas GJ. Flocking in fixed and switching networks. *IEEE Transact Automat Ctrl* 2007; 52: 863–868.
10. La HM and Sheng W. Dynamic target tracking and observing in a mobile sensor network. *Robot Autonom Syst* 2012; 60: 996–1009.
11. Tanner HG. Flocking with obstacle avoidance in switching networks of interconnected vehicles. In: *Proceedings of the 2004 IEEE international conference on robotics and automation*, New Orleans, LA, 26 April–1 May 2004, pp.3006–3011.
12. Tanner HG, Jadbabaie A and Pappas GJ. Stable flocking of mobile agents part II: dynamic topology. In: *Proceedings on the 42nd IEEE conference on decision and control*, Maui, Hawaii, December 2003, vol. 2, pp.2016–2021.
13. Prodan I, Olaru S, Bencatel R, et al. Receding horizon flight control for trajectory tracking of autonomous aerial vehicles. *Control Eng Practice* 2013; 21: 1334–1349.

14. Zhang XY, Duan HB and Yu YX. Receding horizon control for multi-UAVs close formation control based on differential evolution. *Sci China Inform Sci* 2010; 53: 223–235.
15. Zhang XY and Duan HB. Differential evolution-based receding horizon control design for multi-UAVs formation reconfiguration. *Transact Inst Measure Ctrl* 2012; 34: 165–183.
16. Bennet DJ and McInnes CR. Verifiable control of a swarm of unmanned aerial vehicles. *Proc IMechE, Part G: J Aerospace Engineering* 2009; 223: 939–953.
17. Han K, Lee J and Kim Y. Unmanned aerial vehicle swarm control using potential functions and sliding mode control. *Proc IMechE, Part G: J Aerospace Engineering* 2008; 222: 721–730.
18. Ilaya O, Bil C and Evans M. Control design for unmanned aerial vehicle swarming. *Proc IMechE, Part G: J Aerospace Engineering* 2008; 222: 549–567.
19. Lin CL, Li YH and Aouf N. Potential-field-based evolutionary route planner for the control of multiple unmanned aerial vehicles. *Proc IMechE, Part G: J Aerospace Engineering* 2010; 224: 1229–1242.
20. Seo J, Kim Y, Kim S, et al. Consensus-based reconfigurable controller design for unmanned aerial vehicle formation flight. *Proc IMechE, Part G: J Aerospace Engineering* 2012; 226: 817–829.
21. Olfati-Saber R, Fax JA and Murray RM. Consensus and cooperative in networked multi-agent systems. *Proc IEEE* 2007; 95: 215–233.
22. Cao Y, Yu W, Ren W, et al. An overview of recent progress in the study of distributed multi-agent coordination. *IEEE Transact Indus Inform* 2013; 9: 427–438.
23. Ren W. On constrained nonlinear tracking control of a small fixed-wing UAV. *J Intell Robot Syst* 2007; 48: 525–537.
24. Ren J, McIsaac KA and Patel RV. Modified Newton's method applied to potential field-based navigation for mobile robots. *IEEE Transact Robot* 2006; 22: 384–391.
25. Zhang XY, Duan HB and Luo QN. Levenberg-Marquardt based artificial physics method for mobile robot oscillation alleviation. *Sci China Phys Mech Astronom* 2014; 57: 1771–1777.